

# Combinational dual drug delivery system to enhance the care and treatment of gastric cancer patients

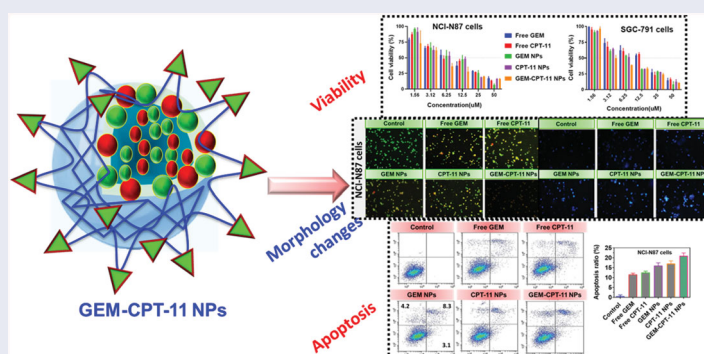
Ying Xiao<sup>a</sup>, Yuewen Gao<sup>b</sup>, Fajuan Li<sup>b</sup> and Zhihe Deng<sup>c</sup>

<sup>a</sup>Second Department of General Surgery, Xinxiang Central Hospital, Xinxiang, PR China; <sup>b</sup>Department of General Surgery, Rizhao People's Hospital, Rizhao, PR China; <sup>c</sup>Department of Gastroenterology, The First Affiliated Hospital of Guangdong Pharmaceutical University, Guangzhou, PR China

## ABSTRACT

Gastric cancer is a frequently occurring cancer with high mortality each year worldwide. Finding new and effective therapeutic strategy against human gastric cancer is still urgently required. Hence, we have established a new method to achieve treatment-actuated modifications in a tumor microenvironment by utilizing synergistic activity between two potential anticancer drugs. Dual drug delivery of gemcitabine (GEM) and Camptothecin-11 (CPT-11) exhibits a great anti-cancer potential, as GEM enhances the effect of CPT-11 treatment of human gastric cells by providing microenvironment stability. However, encapsulation of GEM and CPT-11 obsessed by poly(lactic-co-glycolic acid) (PLGA)-based nanoparticles (NPs) is incompetent owing to unsuitability between the binary free GEM and CPT-11 moieties and the polymeric system. Now, we display that CPT-11 can be prepared by hydrophobic covering of the drug centers with dioleoylphosphatidic acid (DOPA). The DOPA-covered CPT-11 can be co-encapsulated in PLGA NPs alongside GEM to stimulate excellent anticancer property. The occurrence of the CPT-11 suggestively enhanced the encapsulations of GEM into PLGA NPs (GEM-CPT-11 NPs). Formation of the nanocomposite (GEM-CPT-11 NPs) was confirmed by FTIR and X-ray spectroscopic techniques. Further, the morphology of GEM NPs, CPT-11 NPs, and GEM-CPT-11 NPs and NP size was examined by transmission electron microscopy (TEM), respectively. Furthermore, GEM-CPT-11 NPs induced significant apoptosis in human gastric NCI-N87 and SGC-791 cancer cells *in vitro*. The morphological observation and apoptosis were confirmed by the various biochemical assays (AO-EB, nuclear staining, and annexin V-FITC). In addition, evaluation of the hemolysis assay with erythrocytes of human shows excellent biocompatibility of free GEM, free CPT-11, GEM NPs, CPT-11 NPs, and GEM-CPT-11 NPs. The results suggest that GEM-CPT-11 NPs are one of the promising nursing cares for human gastric cancer therapeutic candidates worthy of further investigations.

## GRAPHICAL ABSTRACT



## ARTICLE HISTORY

Received 5 August 2020  
Revised 2 September 2020  
Accepted 8 September 2020


## KEYWORDS

Combinational drug delivery; gastric cancer; nursing care; apoptosis

## 1. Introduction

Gastric cancer is the fourth most common cancer and the second most frequent cause of cancer-associated mortality worldwide. Although many treatment approaches, with maturing endoscopy therapy, chemotherapy, and surgery are used to treat gastric cancer, the results for persistent

progressive gastric cancer are reduced (Yang et al., 2012; Lin et al., 2015; Zheng et al., 2019). The common patients unavoidably die from tumor recurrence or metastasis. Regrettably, till date, no active therapeutic approaches occur to solve this difficult. Hence, the progress of active antitumor agents to resist gastric cancer is a promising field

**CONTACT** Zhihe Deng  [zhihe.d@yahoo.com](mailto:zhihe.d@yahoo.com) No. 19, Nonglinxia Road, Yuexiu District, Guangzhou, China

© 2020 The Author(s). Published by Informa UK Limited, trading as Taylor & Francis Group.

This is an Open Access article distributed under the terms of the Creative Commons Attribution License (<http://creativecommons.org/licenses/by/4.0/>), which permits unrestricted use, distribution, and reproduction in any medium, provided the original work is properly cited.

(Wang et al., 2017; Liang & Yang, 2020; Rong et al., 2020). Also, the drug of selection for the action of gastric cancer, gemcitabine (GEM), suffers from poor extravasation into gastric cancer tissues and rapid enzymatic deamination upon circulation which produces its inactive metabolite, 2',2'-difluorodeoxyuridine (dFdU) (Yan et al., 2019; Konstantinopoulos et al., 2020; Thompson et al., 2020). Moreover, the presence of a desmoplastic stroma around the cancer site creates a barrier for the drug. This results in high dosages of chemotherapy being required to attain an effect, which increases chances of side effects (Li et al., 2015). Thus, significant research efforts have been made toward the design of drug delivery systems targeted at improving the therapeutic outcomes of chemotherapy with GEM and Camptothecin-11 (CPT-11) (Meng et al., 2013; Sobot et al., 2016; Bernards et al., 2018; Jiang et al., 2019).

Combination therapy can be performed via co-administration of a supplementary cancer drug along with a sensitizer. The interfaces within potential anticancer drugs rely on the dose ratios between the two medications and can be potentially incompatible (Sasada et al., 2015; Bang et al., 2017; Jayanathan et al., 2020). Consequently, the importance of preserving a beneficial ratio to maintain a synergistic relationship between two drugs through nanoparticles (NPs) formulations cannot be ignored (Namiki et al., 2011; Wang et al., 2018; Zhu et al., 2020). The procedure of encapsulating several anticancer drugs in individual NPs has proved to be problematic because the drugs have to preserve their important physicochemical properties. Hence, nanoformulations that are prepared by encapsulating numerous medications with varied physico-chemical belongings while preserving controlled ratios are preferred for drug delivery within the body tissues (Yixuan et al., 2010; Li et al., 2012; Xin et al., 2013; Broza et al., 2018).

Nanoparticle-based drug delivery systems have been developed as a valuable system among other important methods for improved malignancy treatment (Ambrogio et al., 2013; Ge & Liu, 2013; Kumar et al., 2013; Florek et al., 2017). Appropriately, structured NPs can isolate the medications from the circulatory system and evade being eliminated by the renal system (Zhang et al., 2018; Li et al., 2019; Zhang et al., 2019, 2020). These NPs have an advanced system to deliver anticancer medications to targeted locations and decrease nonspecific harm to the target tissues, brought about through enhanced permeability and retention (EPR) effects (Zhou et al., 2014; Shen et al., 2016; Chen et al., 2020; Kumari et al., 2020; Martínez-López et al., 2020). Moreover, NP frameworks offer stable watery scattering of medications by surface adjustment and shield medications from degradation, resulting in improved anticancer action (Mirza & Karim, 2019; Ding et al., 2020; Zhou et al., 2020).

In this work, we have described a nanopatform formed by encapsulation of two potential drugs into poly(lactic-co-glycolic acid) (PLGA) nanoparticles (GEM-CPT-11 NPs) via a nanoprecipitation method. Furthermore, *in vitro* cytotoxicity of the drug-loaded NPs was examined in human gastric cancer cells using an MTT assay. Additionally, we examined morphological changes in the treated cells by dual staining

(AO-EB) and nuclear staining methods. Apoptosis was confirmed by the flow cytometry analysis.

## 2. Materials and methods

### 2.1. Materials

CPT-11 and GEM were purchased from TCI (Shanghai, China). Hydrolyzed polyvinyl alcohol (PVA, 85–90%, mol. wt. of 30–50 kDa) was obtained from TCI (Shanghai, China). PLGA polymers (monomer ratio 50:50; MW 7 kDa) were acquired from J&K (Shanghai, China).

### 2.2. Methods

#### 2.2.1. Encapsulation of GEM and CPT-11 in GEM-CPT-11 NPs

An oil/water solvent evaporation technique was adapted to encapsulation of CPT-11 and GEM in PLGA-NPs. Briefly, dioleoylphosphatidic acid (DOPA)-coated CPT-11 (50 µg) cores and GEM (50 µg) were added to a PLGA-NP solution in CHCl<sub>3</sub> (100 mg in 350 µL). The emulsified 9% PVA was mixed into chloroformic solution in 3 mL PBS solutions. The emulsions were stirred for 24 h, and they evaporated the organic solvents. CPT-11- and GEM-loaded PLGA nanoparticles (GEM-CPT-11 NPs) were kept at −20°C to be used for future studies.

A water/oil/water double emulsion solvent evaporation technique was used to fabricate the PLGA-NPs containing DOPA-coated CPT-11, GEM. Briefly, TMR-dextran (200 µL) was blended into a CPT-11 and GEM polymeric solutions in CHCl<sub>3</sub> with sonications. These emulsions were consequently blended in a PVA-PBS solution, left for solvents evaporations (Gupta et al., 2017; Li et al., 2017; Safari et al., 2018; Guo et al., 2019). The emulsions were stirred for 24 h, and they evaporated the organic solvents.

#### 2.3. Examination of *in vitro* drug release

Assessment of *in vitro* drug release kinetics was performed using a dialysis diffusion technique (Chourasiya et al., 2016; Stein et al., 2018; Hsu et al., 2020). GEM-CPT-11 NPs (3 mL), and CPT-11 and GEM (0.1 mg/mL equivalent concentration) solutions were placed into the end-wrapped dialysis covers. Next, they were retained into 20 mL of discharging medium comprising 0.2% Tween-80 in PBS pH 7.4. By stirring at 100 rpm on a detour shakers at 37°C, the drug release medium was removed and an equivalent size of new medium was added. The drug-releasing profiles of CPT-11 and GEM were examined using an UV-vis spectrometer.

#### 2.4. *In vitro* cytotoxicity

NCI-N87 and SGC-791 cells were obtained from the Cell Bank of Beijing (Beijing, China). The cells were maintained in RPMI 1640 culture and Dulbecco's modified Eagle's medium (DMEM) medium supplemented with 10% fetal bovine serum (FBS) and 100 mL<sup>-1</sup> penicillin. Then, NCI-N87 and SGC-791

cells were incubated in a humid atmosphere with 5% CO<sub>2</sub> at 37°C. *In vitro* biochemical staining was obtained from Cell Signaling (Shanghai, China).

### 2.5. Apoptotic staining

The morphological changes of the NCI-N87 and SGC-791 cells were examined by biochemical staining, including acridine orange-ethidium bromide (AO-EB) and Hoechst 33344 staining. After incubating for 24 h, the cells were seeded at a concentration of  $1 \times 10^4$  onto 48-well plates. The cells were treated with free CPT-11, free GEM, CPT-11 NPs, GEM NPs, and GEM-CPT-11 NPs at 2.5 μM concentration for 24 h. On the following day, the staining solution was added. After incubating the plates with the staining solution, the plates were washed with PBS three times. Images were obtained using a fluorescence microscope (Accu Scope EXI-310) at a magnification of  $\times 20$  (Mohamed Subarkhan et al., 2016; Balaji et al., 2020; Deepika et al., 2020).

### 2.6. Flow cytometry/annexin V-PI staining

The flow cytometry examination was examined by using the Apoptosis Detection Kit of fluorescein isothiocyanate (FITC) (Cell Signaling, Shanghai, China) utilized to confirm the apoptotic ratio of NCI-N87 and SGC-791 cells. The cells were treated with free CPT-11, free GEM, CPT-11 NPs, GEM NPs, and GEM-CPT-11 NPs at 2.5 μM concentrations for 24 h. The cells were washed thrice by using trypsin, and suspended in  $1 \times$  binding buffer (500 μL) with FITC Annexin V (5 μL) and of PI (10 μL). After 20 min incubation, the samples were analyzed by flow cytometry. The obtained results were investigated with the BD FACS Canto™ II flow cytometer (Yixuan et al., 2010; Subarkhan & Ramesh, 2016; Mohamed Subarkhan et al., 2018).

### 2.7. Hemocompatibility assay

Human blood samples were obtained from the First Affiliated Hospital of Guangdong Pharmaceutical University. Red blood cells (RBCs) were obtained by centrifuging the samples at 1800 rpm for 5 min at 5°C. The RBCs were washed with PBS three times and resuspended in 4 mL of

PBS. Next, 0.1 mL of diluted RBCs was added to the free GEM, free CPT-11, GEM NPs, CPT-11 NPs, and GEM-CPT-11 NPs in 0.5 mL PBS suspension at the corresponding concentrations and incubated for 4 h. After incubation, the samples were transferred onto 96-well plates. Hemolytic activity was determined by measuring at an absorbance of 570 nm. The control samples of the lyses buffer and 100% lyses buffer were also analyzed in these experimental procedures (Tramer et al., 2012; Evans et al., 2013; Liang et al., 2019; Mohamed Subarkhan et al., 2019). The proportion of hemolysis was determined as follows: % hemolysis =  $(A_s - A_n) / (A_p - A_n) \times 100\%$ , where  $A_s$  denotes the absorbance of samples (free GEM, free CPT-11, GEM NPs, CPT-11 NPs, and GEM-CPT-11 NPs) at various concentrations (5, 10, 15, 20, and 25), and  $A_n$  and  $A_p$  denote the negative and positive controls, respectively.

## 3. Results and discussion

### 3.1. Structural morphology and characterization

Our achievement in proficiently stacking of CPT-11 (CPT-11) and GEM (GEM) into PLGA-NPs (designated as GEM-CPT-11 NPs) proposes another chance to co-deliver two medications for blend treatment. For instance, hydrophobic CPT-11 and GEM can be built into GEM-CPT-11 NPs simultaneously with other hydrophobic antitumor medications, such as GEM and paclitaxel. GEM was preferred for this study and its centers were embodied into GEM-CPT-11 NPs close to CPT-11, because of its cooperative energy with CPT-11. The main procedure of stacking of GEM and CPT-11 inside GEM-CPT-11 NPs is shown in Figure 1. GEM and CPT-11 are incorporated in the polymer framework of GEM-CPT-11 NPs done by hydrophobic interaction. Hence, the insertions are restricted by similarities concerning GEM and CPT-11 and their hydrophobic interaction with the co-polymer. Self-assembled nanoparticles (GEM-CPT-11 NPs) were formed spontaneously with 4 mg/mL CPT-11 and 8 mg/mL GEM by employing intermolecular hydrophobic interactions between the lipophilic moiety of GEM and CPT-11, as depicted in Figure 1.

The effects of the morphological surface of the hydrothermally prepared GEM NPs, CPT-11 NPs, and GEM-CPT-11 NPs were investigated through TEM analysis. The results as

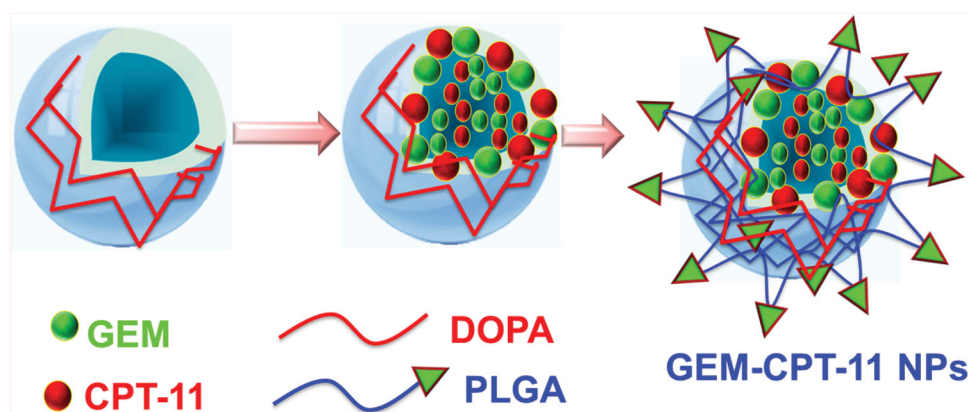
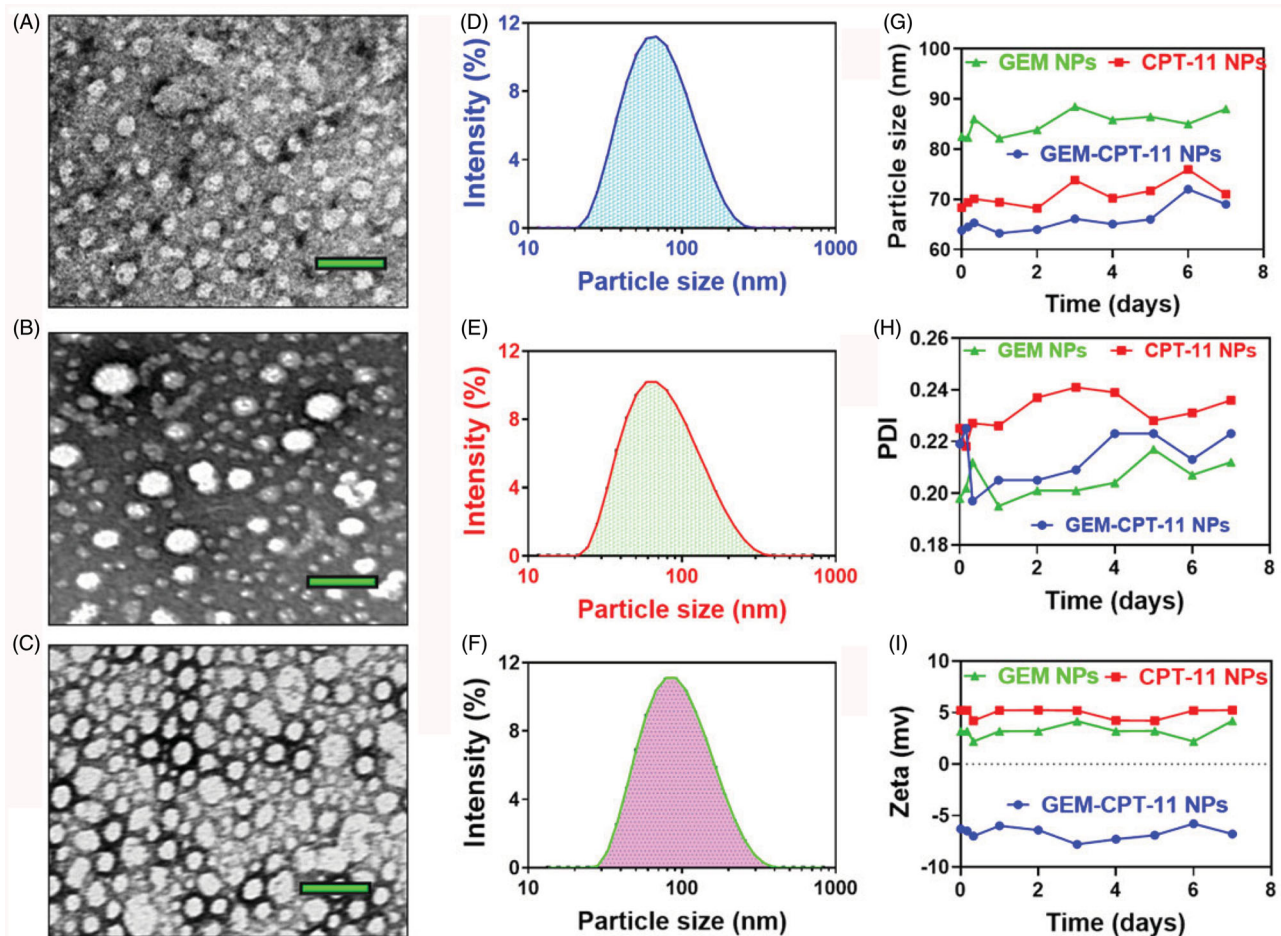
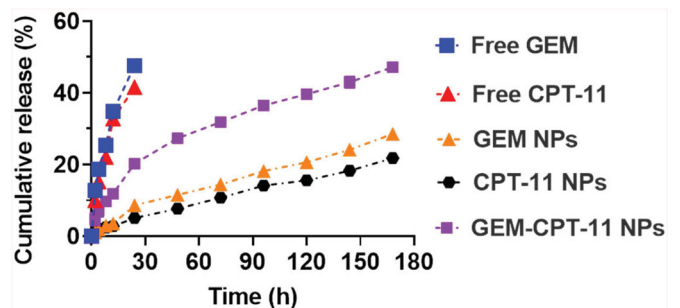


Figure 1. A schematic of the self-assembly of GEM and CPT-11 to form GEM-CPT-11 NPs of the treatment of gastric cancer.



**Figure 2.** Characterization of the nanoparticles. (A–F) Morphology and particle size of GEM NPs, CPT-11 NPs, and GEM-CPT-11 NPs under a transmission electron microscope after negative staining with sodium phosphotungstate solution (2%, w/v). Scale bar: 20 nm. Particle size distribution of GEM NPs, CPT-11 NPs, and GEM-CPT-11 NPs analyzed by dynamic light scattering via a Zetasizer. (G–I) Stability of the GEM NPs, CPT-11 NPs, and GEM-CPT-11 examined by the dynamic light scattering.

shown in Figure 2(A–C) depicts the creation of GEM-CPT-11 NPs. Additionally, morphological changes the synthesized polymeric NPs that were analyzed by HR-TEM. The nanocomposite was composed of agglomerated clusters of well-shaped hydroxyapatite nanocomposites (Figure 2(A–C)). The size of the GEM-CPT-11 NPs was examined by dynamic light scattering (DLS) analysis. The diameters of GEM NPs, CPT-11 NPs, and GEM-CPT-11 NPs measured from TEM images were in the range of  $63.9 \pm 0.3$ ,  $68.7 \pm 0.5$ ,  $81.2 \pm 0.9$  nm (Figure 2(D–F)) and the polyplexes index was  $0.277 \pm 0.05$ ,  $0.252 \pm 0.05$ , and  $0.159 \pm 0.02$  for GEM NPs, CPT-11 NPs, and GEM-CPT-11 NPs, respectively, which is in agreement with the results of light scattering measurements and gives clear evidence of the size of the NPs compared to those analyses by TEM (Figure 2(D–F)). The stability of the GEM NPs, CPT-11 NPs, and GEM-CPT-11 NPs in PBS media was examined by determining the particle size of the GEM NPs, CPT-11 NPs, and GEM-CPT-11 NPs by DLS. Polyplexes index, specifically GEM NPs, CPT-11 NPs, and GEM-CPT-11 NPs, at an NPs ratio of 100:1 was organized and incubated for 30 min at  $37^\circ\text{C}$  in order to confirm complete polyplex formation (Figure 2(G,H)). All the experiments were repeated three times. Additionally, the zeta potential and the stability of GEM NPs,



**Figure 3.** Drug release profiles (GEM and CPT-11) from the GEM NPs, CPT-11 NPs, and GEM-CPT-11 NPs against PBS containing 0.3% polysorbate 80.

CPT-11 NPs, and GEM-CPT-11 were determined to be  $5.2 \pm 0.4$ ,  $6.8 \pm 0.5$ , and  $-6.3 \pm 0.3$  mV (Figure 2(I)) by DLS.

### 3.2. Controlled release of GEM-CPT-11 NPs

Controlled release of GEM-CPT-11 NPs plays a vital role in the size, solubility, degradation, and drug loading by the NP frameworks. It is predictable that results confirm the drug release profile which shows the CPT-11 + GEM-loaded GEM-CPT-11 NPs reserve an enhanced efficiency to the

frameworks. In contrast, if the drugs not received, a reckless and undesired untimely discharge will occur. These methods provide clues to the production of shell holes that permit the discharge of drugs. The controlled drug release was

measured via physical and chemical analyses of the GEM-CPT-11 NPs and the encapsulation properties of the drugs. These dialysis methods were utilized to examine the outcomes of controlled release of the drugs encapsulated in the

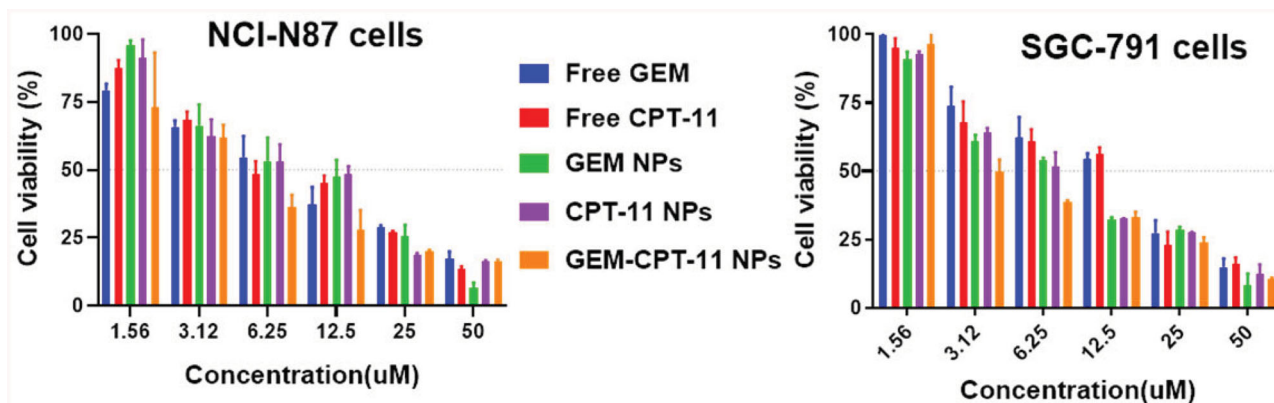


**Figure 4.** *In vitro* cytotoxicity of free CPT-11, free GEM, CPT-11 NPs, GEM NPs, and GEM-CPT-11 NPs were evaluated in NCI-N87 and SGC-791 gastric cancer cells. Cell viability was examined by the MTT assay after 24 h of drug incubation.

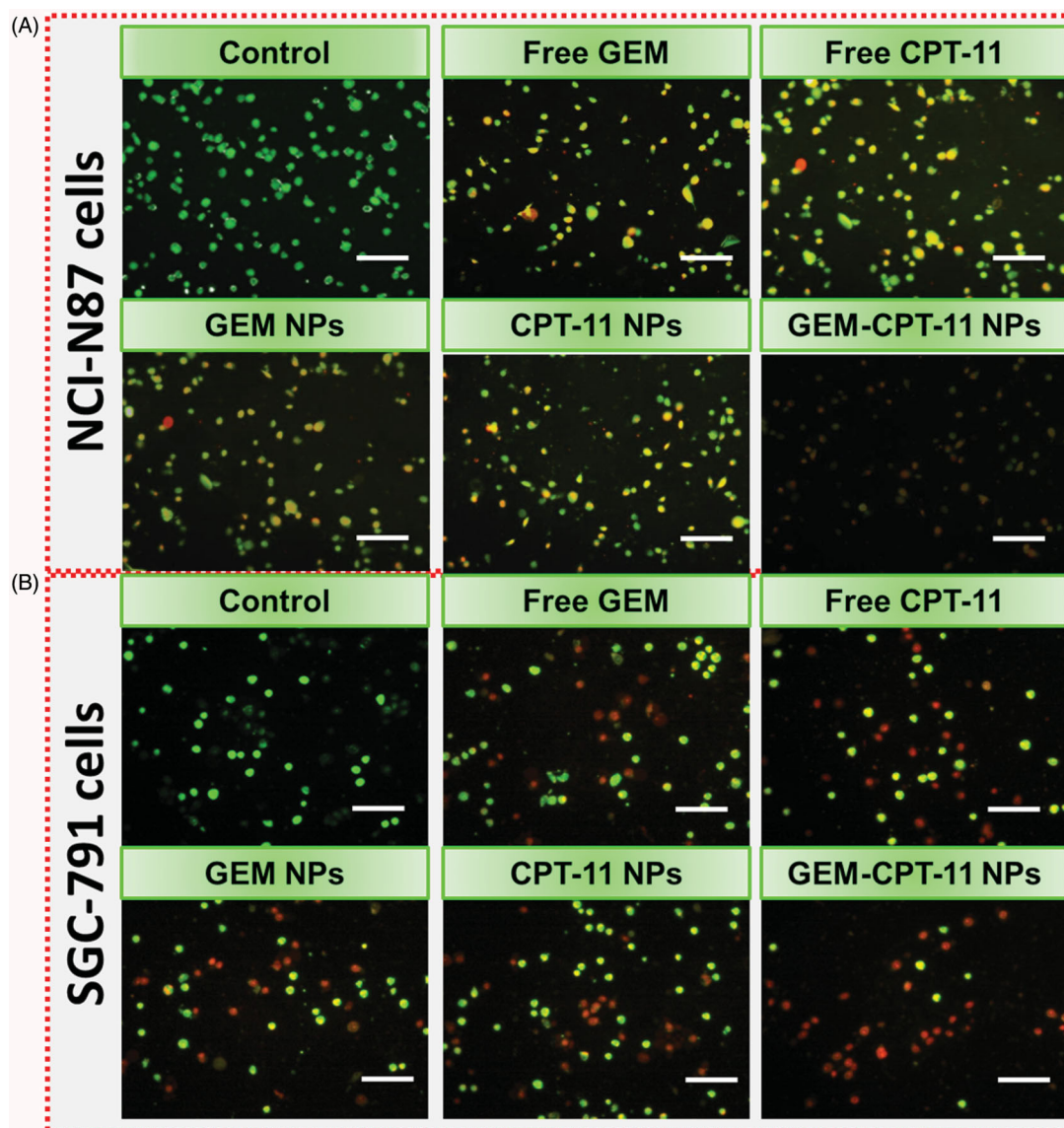


**Figure 5.** Dual AO/EB staining assay for examining free CPT-11, free GEM, CPT-11 NPs, GEM NPs, and GEM-CPT-11 NPs-induced cell death in NCI-N87 (A) and SGC-791 (B) cells. The cells were treated with free CPT-11, free GEM, CPT-11 NPs, GEM NPs, and GEM-CPT-11 NPs at 2.5 μM concentration for 24 h. Scale bar 20 μM.

GEM-CPT-11 NPs and those associated with the free CPT-11 and GEM. The controlled release experiment was conducted in PBS at a pH of 7.2 at 37 °C. The controlled release profiles of the combination of CPT-11 and GEM loaded in the GEM-CPT-11 NPs displayed an initial release in about 5 h monitored via sluggish release for six days (Figure 3). First 10 h, half of the CPT-11 and GEM was discharged after the GEM-CPT-11 NPs formations. Subsequently, later 24 h, a gentle release of 40–50% was observed. These results indicate that the conjugation of CPT-11 and GEM on the surface of the PLGA-NPs (GEM-CPT-11 NPs) did not show any adverse effect on the controlled release by these nanocomposites.

### 3.3. In vitro cytotoxicity

After successful synthesis of GEM-CPT-11 NPs, we performed an MTT assay to evaluate the cytotoxic effects of free CPT-11, free GEM, CPT-11 NPs, GEM NPs, and GEM-CPT-11 NPs on gastric cancer cell lines, comprising NCI-N87 and SGC-791 cancer cells. Following treatments with the medications for 24 h, the cell viability was monitored, and minimum-inhibitory concentrations (IC<sub>50</sub>) were obtained from the dose-dependent curve (Figure 4). Surprisingly, GEM-CPT-11 NPs

displayed substantial improvement in cytotoxicity of the cancer cells. For instance, in NCI-N87 cell lines, IC<sub>50</sub> of 10.91 ± 11.12, 10.35 ± 1.22, 9.05 ± 2.11, 9.46 ± 0.98, and 6.62 ± 0.97 was observed for free CPT-11, free GEM, CPT-11 NPs, GEM NPs, and GEM-CPT-11 NPs, respectively. In SGC-791 cell lines, IC<sub>50</sub> of 19.27 ± 3.30, 17.70 ± 2.54, 11.20 ± 0.98, 10.22 ± 1.87, and 7.16 ± 2.80 for free CPT-11, free GEM, CPT-11 NPs, GEM NPs, and GEM-CPT-11 NPs was observed, respectively. The enhanced cytotoxicity of the GEM-CPT-11 NPs was owing to the entire release of the double potential anticancer medications into the tumor cells. The hydrophilic molecules of PLGA dispense the aqueous layer via a lipid bilayer for cell membrane penetration. Thus, the enhancement of cellular uptake requires the cell membrane nucleosides delivery for the proteins.

### 3.4. Morphological changes in NCI-N87 and SGC-791 human gastric cancer cells

Dual staining AO-EB is a qualitative technique used to identify live, early, late apoptotic, and necrotic cancer cells using fluorescent images to observe morphological changes in the nucleus of cells (Kasibhatla et al., 2006; Liu et al., 2015;

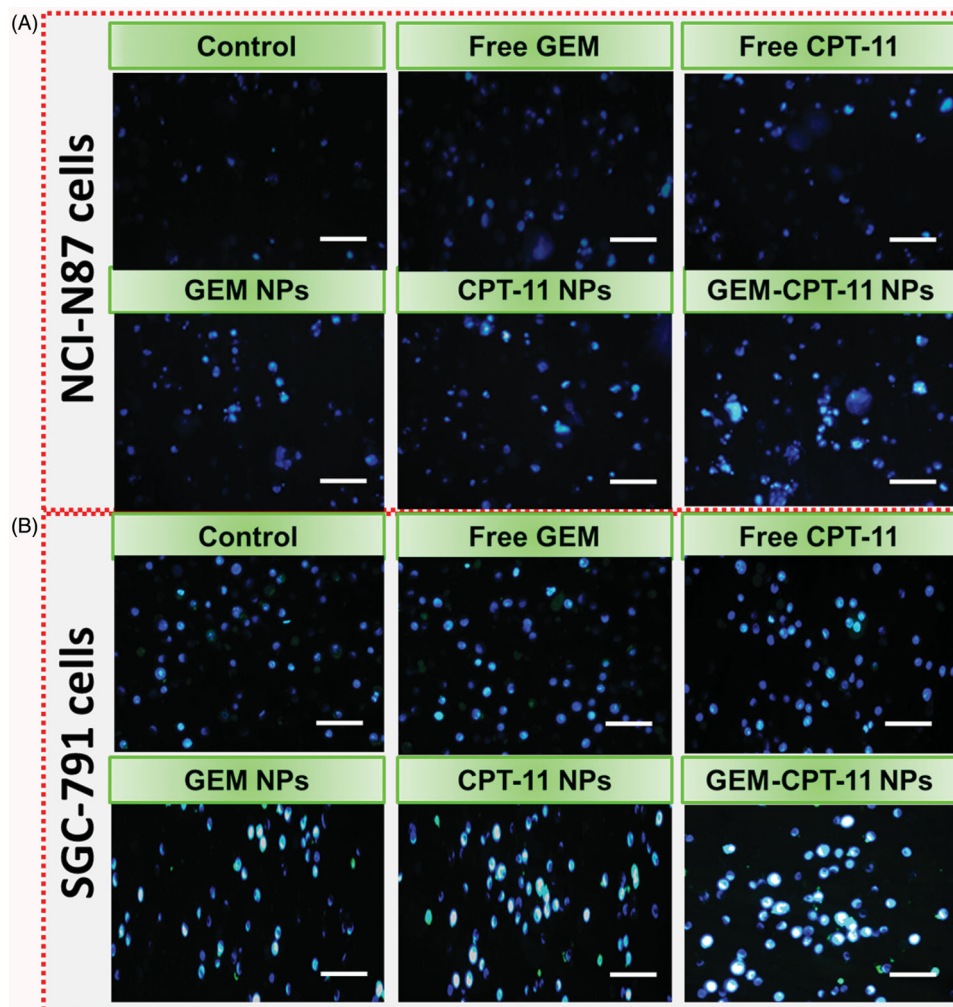


**Figure 6.** Nuclear (Hoechst 33258) staining assay for examining free CPT-11, free GEM, CPT-11 NPs, GEM NPs, and GEM-CPT-11 NPs-induced cell death in NCI-N87 (A) and SGC-791 (B) cells. The cells were treated with free CPT-11, free GEM, CPT-11 NPs, GEM NPs, and GEM-CPT-11 NPs at 2.5 μM concentration for 24 h. Scale bar 20 μM.

Tambe et al., 2018). AO permeates the intact membranes of usual and early apoptotic cell and binds to DNA, which fluoresces uniform green in normal cells and as patches in early apoptotic cells due to chromatin condensations. In difference, EB is only penetrable in the incapacitated membrane of late apoptotics and necrotics cell, where it fluoresces as bright orange patch through its bindings to DNA fragment or apoptotic moiety in late apoptotic cells, and as a unchanging orange fluorescence in the necrotic cell, as it has the nuclear changes in the morphology of viable cell. AO-EB-stained NCI-N87 and SGC-791 cells were incubated with free CPT-11, free GEM, CPT-11 NPs, GEM NPs, and GEM-CPT-11 NPs for 24 h. As presented in Figure 5, the presence of orange with reddish fluorescence with chromatin fragmentation after treatment of NCI-N87 and SGC-791 cells treated with free CPT-11, free GEM, CPT-11 NPs, GEM NPs, and GEM-CPT-11 NPs suggested that the GEM-CPT-11 NPs largely induced apoptosis in NCI-N87 and SGC-791 cells.

Hoechst 33258 staining was used to observe chromatin fragmentation, bi- and/or multinucleation, cytoplasmic vacuolation, nuclear swelling, cytoplasmic bleating, and late apoptosis in gastric cancer cells by visualizing dot-like chromatin condensation. Hoechst-33258-stained NCI-N87 and SGC-791 cells were incubated with free CPT-11, free GEM, CPT-11 NPs, GEM NPs, and GEM-CPT-11 NPs for 24 h. As displayed in Figure 6, the presence of blue fluorescence with chromatin condensation after treatment of NCI-N87 and SGC-791 cells treated with free CPT-11, free GEM, CPT-11 NPs, and GEM NPs suggested that the GEM-CPT-11 NPs largely induced apoptosis in NCI-N87 and SGC-791 (Figure 6).

### 3.5. Apoptosis in NCI-N87 and SGC-791 human gastric cancer cells

Apoptosis may be reckoned as an important obstacle for a damaged cell to become malignant tumors. Since the

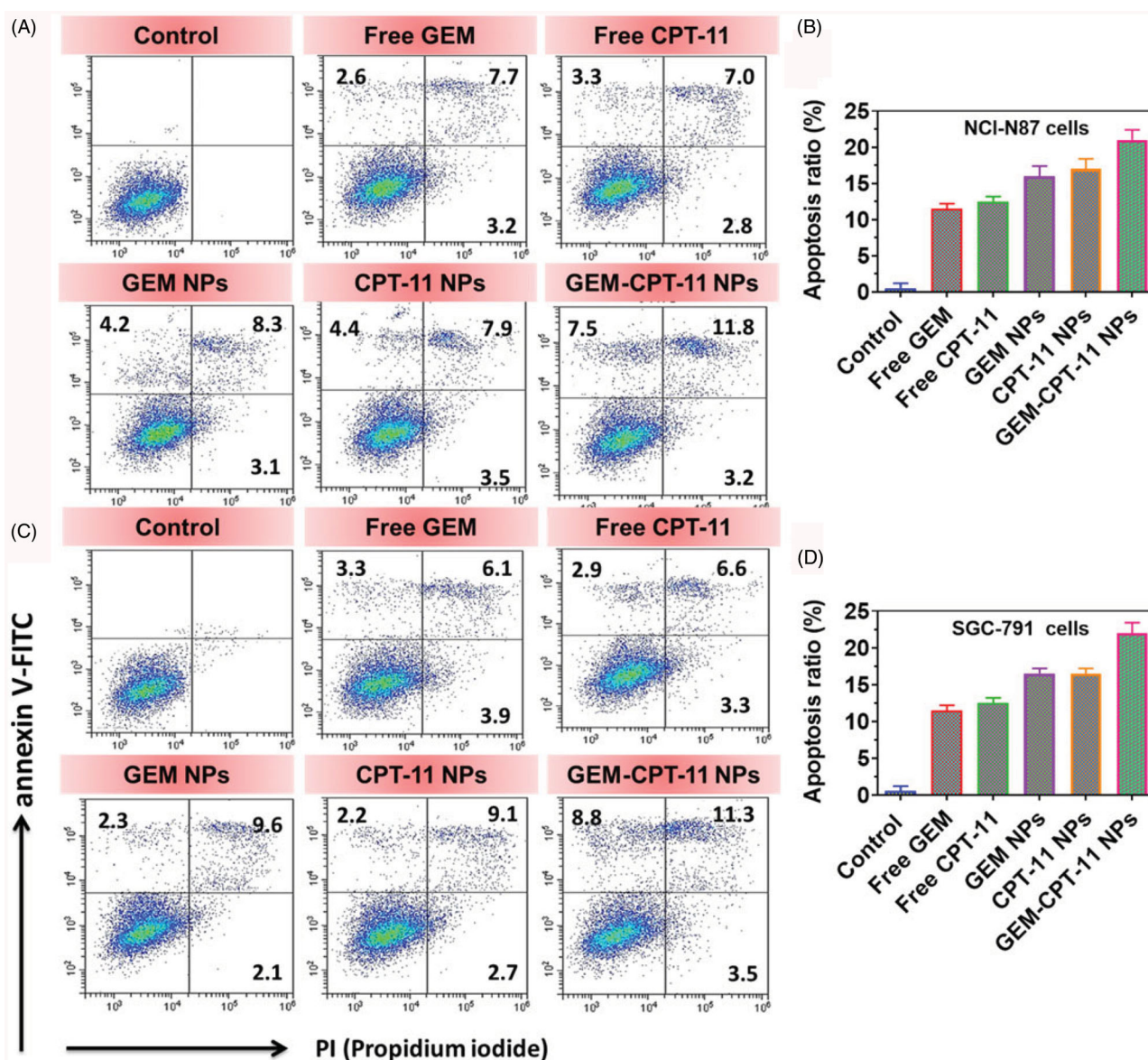


**Figure 7.** (A, C) Apoptotic analysis of NCI-N87 and SGC-791 cells using flow cytometry. The cells were treated with free CPT-11, free GEM, CPT-11 NPs, GEM NPs, and GEM-CPT-11 NPs at 2.5 μM concentration for 24 h and then stained with FITC annexin V/PI for flow cytometry analysis. (B, D) Apoptosis ratio of NCI-N87 and SGC-791 cells.

complexes promote apoptosis induction in cancer cells, flow cytometry using annexin V-FITC/propidium iodide (PI) double staining was carried out for the quantitative discrimination of apoptotic cells (Rehana et al., 2017; Mohan et al., 2018; Sathiya Kamatchi et al., 2020). Phosphatidylserine (PS) is a cell cycle signaling phospholipid located inner side of the membrane of a healthy cell but is reverted to the outer membrane for recognition by neighboring cells at the time of apoptosis. Hence, the translocation of PS is a morphological hallmark of apoptosis and can be spotted by its binding with fluorescently labeled annexin V which in turn detected by flow cytometry. Further, the addition of PI to annexin V stained cells is used to discriminate and concomitantly quantify the live cells (lower left quadrant-annexin V(-)/PI(-)), early apoptotic cells (upper left quadrant-annexin V(+)/PI(-)) and late apoptotic cells (upper right quadrant-annexin V(+)/PI(+)) using FACS. As projected in Figure 7, the incubation of free CPT-11, free GEM, CPT-11 NPs, GEM NPs, and GEM-CPT-11 NPs with NCI-N87 and SGC-791 cells conspicuously induced apoptosis. It is worth to note that the titled complexes induce apoptosis even at very low concentrations which are less than their  $IC_{50}$ . In comparison with control, the

cell population was higher (6–9%) in annexin V(+)/PI(-) (upper left) quadrant indicating the induction of early apoptosis. This effect was ascertained to be high for GEM-CPT-11 NPs than the free CPT-11, free GEM, CPT-11 NPs, GEM NPs analogous with the results of MTT, and AO-EB staining assays. It is to note that the test samples displayed comparatively better apoptotic induction on NCI-N87 and SGC-791 cells.

### 3.6. Hemolysis assay in NCI-N87 and SGC-791 human gastric cancer cells

The analysis of the interaction between NPs and human blood erythrocytes using hemolysis assays is the key in determining the blood compatibility of NPs (Figure 8). Free GEM, free CPT-11, GEM NPs, CPT-11 NPs, and GEM-CPT-11 NPs were found to display excellent biocompatibility with human RBCs, as shown in Figure 8. The role of the toxic substances appeared to be nano-specific. According to the IOS/Technical Report 7406, the hemolytic rate of NPs or materials is limited to 5%. The release of erythrocytes by Free GEM, free CPT-11, GEM NPs, CPT-11 NPs, and GEM-CPT-11 NPs was

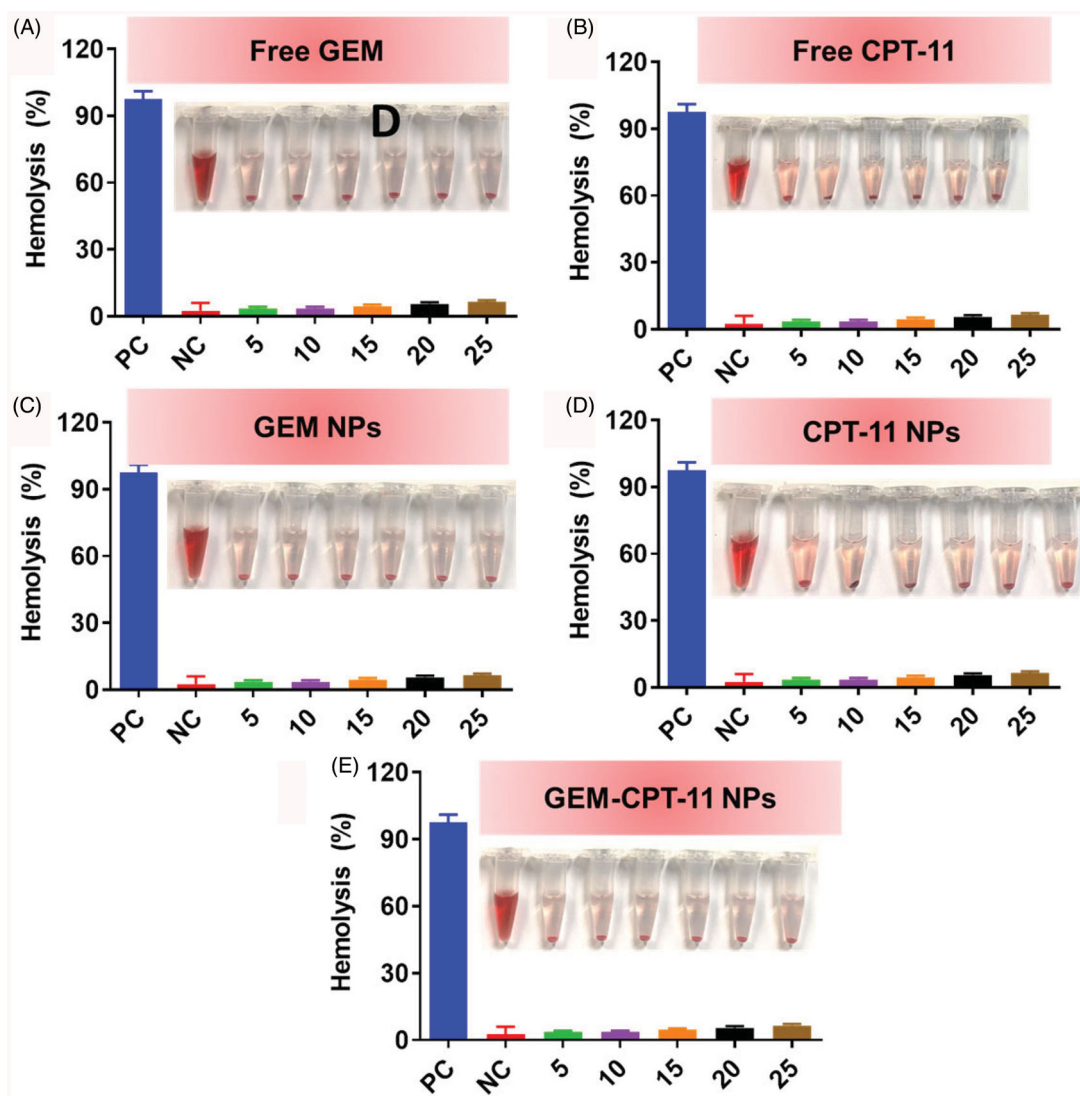


Figure 8. Biocompatibility of free CPT-11, free GEM, CPT-11 NPs, GEM NPs, and GEM-CPT-11 NPs with human blood.



insignificant, indicating that the NPs had a negligible level of toxicity, and thus, they were safe to cells.

#### 4. Conclusions

We developed GEM-CPT-11 NPs by encapsulating GEM and CPT-11 moieties to change the tumor microenvironment for improved drug accretion and additional anticancer activities. At first, CPT-11 was incorporated into GEM-CPT-11 NPs with effectual loading and encapsulation by direct self-assembly method. In this study, we showed that CPT-11 could be made hydrophobic by using an oil/water solvent evaporation method for drug delivery. These DOPA-covered CPT-11 centers were compatible with PLGA and could be co-encapsulated in GEM-CPT-11 NPs. The closeness of the CPT-11 centers fundamentally developed the epitome of GEM into PLGA-NPs. The formation of the nanocomposite was confirmed by FTIR and X-ray spectroscopic techniques. Further, TEM electroscopic techniques displayed the crystallized structure of the nanocomposite. GEM-CPT-11 NPs comprising double CPT-11 and GEM led to remarkable apoptosis in human gastric NCI-N87 and SGC-791 cancer cells. Further, morphological changes in the cells were monitored using dual staining and nuclear staining methods. AO-EB fluorescent staining and flow cytometry analysis reveal that all the complexes induce cancer cell death by apoptosis mechanism. Additionally, evaluation of the hemolysis assay with erythrocytes of human shows excellent biocompatibility of free GEM, free CPT-11, GEM NPs, CPT-11 NPs, and GEM-CPT-11 NPs. The preliminary results of the work established further investigation of the nursing cares *in vivo* examinations in future.

#### Disclosure statement

No potential conflict of interest was reported by the author(s).

#### References

- Ambrogio MW, Frasconi M, Yilmaz MD, Chen X. (2013). New methods for improved characterization of silica nanoparticle-based drug delivery systems. *Langmuir* 29:15386–93.
- Balaji S, Mohamed Subarkhan MK, Ramesh R, et al. (2020). Synthesis and structure of arene Ru(II) N<sub>3</sub>O-chelating complexes: *in vitro* cytotoxicity and cancer cell death mechanism. *Organometallics* 39:1366–75.
- Bang Y-J, Xu R-H, Chin K, et al. (2017). Olaparib in combination with paclitaxel in patients with advanced gastric cancer who have progressed following first-line therapy (GOLD): a double-blind, randomised, placebo-controlled, phase 3 trial. *Lancet Oncol* 18:1637–51.
- Bernards N, Ventura M, Fricke IB, et al. (2018). Liposomal irinotecan achieves significant survival and tumor burden control in a triple negative breast cancer model of spontaneous metastasis. *Mol Pharm* 15:4132–8.
- Broza YY, Vishinkin R, Barash O, et al. (2018). Synergy between nanomaterials and volatile organic compounds for non-invasive medical evaluation. *Chem Soc Rev* 47:4781–859.
- Chen Z, Wan L, Yuan Y, et al. (2020). pH/GSH-dual-sensitive hollow mesoporous silica nanoparticle-based drug delivery system for targeted cancer therapy. *ACS Biomater Sci Eng* 6:3375–87.
- Chourasiya V, Bohrey S, Pandey A. (2016). Formulation, optimization, characterization and *in-vitro* drug release kinetics of atenolol loaded PLGA nanoparticles using 33 factorial design for oral delivery. *Mater Discover* 5:1–13.
- Deepika MS, Thangam R, Sundarraj S, et al. (2020). Co-delivery of diverse therapeutic compounds using PEG–PLGA nanoparticle cargo against drug-resistant bacteria: an improved anti-biofilm strategy. *ACS Appl Bio Mater* 3:385–99.
- Ding S, Khan AI, Cai X, et al. (2020). Overcoming blood–brain barrier transport: advances in nanoparticle-based drug delivery strategies. *Mater Today* 37:112–25.
- Evans BC, Nelson CE, Yu SS, et al. (2013). *Ex vivo* red blood cell hemolysis assay for the evaluation of pH-responsive endosomolytic agents for cytosolic delivery of biomacromolecular drugs. *J Vis Exp* e50166.
- Florek J, Caillard R, Kleitz F. (2017). Evaluation of mesoporous silica nanoparticles for oral drug delivery – current status and perspective of MSNs drug carriers. *Nanoscale* 9:15252–77.
- Ge Z, Liu S. (2013). Functional block copolymer assemblies responsive to tumor and intracellular microenvironments for site-specific drug delivery and enhanced imaging performance. *Chem Soc Rev* 42:7289–325.
- Guo X-S, Zhang Z-K, Zhang T-Y, et al. (2019). Interfacial self-assembly of amphiphilic conjugated block copolymer into 2D nanotapes. *Soft Matter* 15:8790–9.
- Gupta RK, Dunderdale GJ, England MW, Hozumi A. (2017). Oil/water separation techniques: a review of recent progresses and future directions. *J Mater Chem A* 5:16025–58.
- Hsu M-Y, Huang Y-T, Weng C-J, et al. (2020). Preparation and *in vitro/in vivo* evaluation of doxorubicin-loaded poly[lactide-co-glycolic acid] microspheres using electrospray method for sustained drug delivery and potential intratumoral injection. *Colloids Surf B Biointerfaces* 190: 110937.
- Jayanathan M, Erwin RP, Molacek N, et al. (2020). MAGIC versus MacDonald treatment regimens for gastric cancer: trends and predictors of multimodal therapy for gastric cancer using the National Cancer Database. *Am J Surg* 219:129–35.
- Jiang Z, Pflug K, Usama SM, et al. (2019). Cyanine–gemcitabine conjugates as targeted theranostic agents for glioblastoma tumor cells. *J Med Chem* 62:9236–45.
- Kasibhatla S, Amarante-Mendes GP, Finucane D, et al. (2006). Acridine orange/ethidium bromide (AO/EB) staining to detect apoptosis. *CSH Protoc* 2006:799–803.
- Konstantinopoulos PA, Cheng S-C, Wahner Hendrickson AE, et al. (2020). Berzosertib plus gemcitabine versus gemcitabine alone in platinum-resistant high-grade serous ovarian cancer: a multicentre, open-label, randomised, phase 2 trial. *Lancet Oncol* 21:957–68.
- Kumar A, Chen F, Mozhi A, et al. (2013). Innovative pharmaceutical development based on unique properties of nanoscale delivery formulation. *Nanoscale* 5:8307–25.
- Kumari R, Sunil D, Ningthoujam RS. (2020). Hypoxia-responsive nanoparticle based drug delivery systems in cancer therapy: an up-to-date review. *J Control Release* 319:135–56.
- Li H, Li S, Li Z, et al. (2017). Polysulfone/SiO<sub>2</sub> hybrid shell microcapsules synthesized by the combination of pickering emulsification and the solvent evaporation technique and their application in self-lubricating composites. *Langmuir* 33:14149–55.
- Li Q, Zhang D, Zhang J, et al. (2019). A three-in-one immunotherapy nanoweapon via cascade-amplifying cancer-immunity cycle against tumor metastasis, relapse, and postsurgical regrowth. *Nano Lett* 19: 6647–57.
- Li X, Lu X, Xu H, et al. (2012). Paclitaxel/tetrandrine coloaded nanoparticles effectively promote the apoptosis of gastric cancer cells based on “oxidation therapy”. *Mol Pharm* 9:222–9.
- Li X, Wang X, Xu C, et al. (2015). Synthesis and biological evaluation of nitric oxide-releasing hybrids from gemcitabine and phenylsulfonyl furoxans as anti-tumor agents. *Med Chem Commun* 6:1130–6.
- Liang J-R, Yang H. (2020). Ginkgolic acid (GA) suppresses gastric cancer growth by inducing apoptosis and suppressing STAT3/JAK2 signaling regulated by ROS. *Biomed Pharmacother* 125:109585.
- Liang Y, Zhao X, Hu T, et al. (2019). Mussel-inspired, antibacterial, conductive, antioxidant, injectable composite hydrogel wound dressing to promote the regeneration of infected skin. *J Colloid Interface Sci* 556:514–28.

- Lin Y-H, Chen Z-R, Lai C-H, et al. (2015). Active targeted nanoparticles for oral administration of gastric cancer therapy. *Biomacromolecules* 16: 3021–32.
- Liu K, Liu P, Liu R, Wu X. (2015). Dual AO/EB staining to detect apoptosis in osteosarcoma cells compared with flow cytometry. *Med Sci Monit Basic Res* 21:15–20.
- Martínez-López AL, Pangua C, Reboredo C, et al. (2020). Protein-based nanoparticles for drug delivery purposes. *Int J Pharm* 581:119289.
- Meng H, Zhao Y, Dong J, et al. (2013). Two-wave nanotherapy to target the stroma and optimize gemcitabine delivery to a human pancreatic cancer model in mice. *ACS Nano* 7:10048–65.
- Mirza Z, Karim S. (2019). Nanoparticles-based drug delivery and gene therapy for breast cancer: recent advancements and future challenges. *Semin Cancer Biol*.
- Mohamed Subarkhan MK, Ramesh R, Liu Y. (2016). Synthesis and molecular structure of arene ruthenium(II) benzhydrazone complexes: impact of substitution at the chelating ligand and arene moiety on antiproliferative activity. *New J Chem* 40:9813–23.
- Mohamed Subarkhan MK, Ren L, Xie B, et al. (2019). Novel tetranuclear ruthenium(II) arene complexes showing potent cytotoxic and antimetastatic activity as well as low toxicity in vivo. *Eur J Med Chem* 179: 246–56.
- Mohan N, Mohamed Subarkhan MK, Ramesh R. (2018). Synthesis, antiproliferative activity and apoptosis-promoting effects of arene ruthenium(II) complexes with N, O chelating ligands. *J Organomet Chem* 859:124–31.
- Mohamed Subarkhan M, Sundar S, Rengan R. (2018). Synthesis and structure of new binuclear ruthenium(II) arene benzil bis(benzoylhydrazon) complexes: investigation on antiproliferative activity and apoptosis induction. *Inorg Chem Front* 5:585–96.
- Namiki Y, Fuchigami T, Tada N, et al. (2011). Nanomedicine for cancer: lipid-based nanostructures for drug delivery and monitoring. *Acc Chem Res* 44:1080–93.
- Rehana D, Mahendiran D, Kumar RS, Rahiman AK. (2017). Evaluation of antioxidant and anticancer activity of copper oxide nanoparticles synthesized using medicinally important plant extracts. *Biomed Pharmacother* 89:1067–77.
- Rong L, Li Z, Leng X, et al. (2020). Salidroside induces apoptosis and protective autophagy in human gastric cancer AGS cells through the PI3K/Akt/mTOR pathway. *Biomed Pharmacother* 122:109726.
- Safari H, Adili R, Holinstat M, Eniola-Adefeso O. (2018). Modified two-step emulsion solvent evaporation technique for fabricating biodegradable rod-shaped particles in the submicron size range. *J Colloid Interface Sci* 518:174–83.
- Sasada A, Takagi M, Tabata S, et al. (2015). A patient with stage IV gastric cancer who acquired complete remission after undergoing multi-peptide dendritic cell immunotherapy in combination with standard therapies. *Personal Med Univ* 4:70–2.
- Sathiya Kamatchi T, Mohamed Subarkhan MK, Ramesh R, et al. (2020). Investigation into antiproliferative activity and apoptosis mechanism of new arene Ru(II) carbazole-based hydrazone complexes. *Dalton Trans* 49:11385–95.
- Shen B, Ma Y, Yu S, Ji C. (2016). Smart multifunctional magnetic nanoparticle-based drug delivery system for cancer thermo-chemotherapy and intracellular imaging. *ACS Appl Mater Interfaces* 8:24502–8.
- Sobot D, Mura S, Couvreur P. (2016). How can nanomedicines overcome cellular-based anticancer drug resistance? *J Mater Chem B* 4: 5078–100.
- Stein S, Auel T, Kempin W, et al. (2018). Influence of the test method on in vitro drug release from intravitreal model implants containing dexamethasone or fluorescein sodium in poly(D,L-lactide-co-glycolide) or polycaprolactone. *Eur J Pharm Biopharm* 127:270–8.
- Subarkhan MKM, Ramesh R. (2016). Ruthenium(II) arene complexes containing benzhydrazone ligands: synthesis, structure and antiproliferative activity. *Inorg Chem Front* 3:1245–55.
- Tambe P, Kumar P, Paknikar KM, Gajbhiye V. (2018). Decapeptide functionalized targeted mesoporous silica nanoparticles with doxorubicin exhibit enhanced apoptotic effect in breast and prostate cancer cells. *Int J Nanomedicine* 13:7669–80.
- Thompson BR, Shi J, Zhu H-J, Smith DE. (2020). Pharmacokinetics of gemcitabine and its amino acid ester prodrug following intravenous and oral administrations in mice. *Biochem Pharmacol* 180:114127.
- Tramer F, Da Ros T, Passamonti S. (2012). Screening of fullerene toxicity by hemolysis assay. *Methods Mol Biol* 926:203–17.
- Wang X-P, Wang Q-X, Lin H-P, Chang N. (2017). Anti-tumor bioactivities of curcumin on mice loaded with gastric carcinoma. *Food Funct* 8: 3319–26.
- Wang Y, Wang F, Shen Y, et al. (2018). Tumor-specific disintegratable nanohybrids containing ultrasmall inorganic nanoparticles: from design and improved properties to cancer applications. *Mater Horiz* 5: 184–205.
- Xin J, Zhang X, Liang J, et al. (2013). In vivo gastric cancer targeting and imaging using novel symmetric cyanine dye-conjugated GX1 peptide probes. *Bioconjug Chem* 24:1134–43.
- Yan L, Liu G, Cao H, et al. (2019). Hsa\_circ\_0035483 sponges hsa-miR-335 to promote the gemcitabine-resistance of human renal cancer cells by autophagy regulation. *Biochem Biophys Res Commun* 519: 172–8.
- Yang Y, Toy W, Choong LY, et al. (2012). Discovery of SLC3A2 cell membrane protein as a potential gastric cancer biomarker: implications in molecular imaging. *J Proteome Res* 11:5736–47.
- Yixuan Y, Kiat LS, Yee CL, et al. (2010). Cathepsin S mediates gastric cancer cell migration and invasion via a putative network of metastasis-associated proteins. *J Proteome Res* 9:4767–78.
- Zhang D, Zhang J, Li Q, et al. (2019). Cold to hot: rational design of a minimalist multifunctional photo-immunotherapy nanoplatform toward boosting immunotherapy capability. *ACS Appl Mater Interfaces* 11:32633–46.
- Zhang H, Li Q, Liu R, et al. (2018). A versatile prodrug strategy to in situ encapsulate drugs in MOF nanocarriers: a case of cytarabine-IR820 prodrug encapsulated ZIF-8 toward chemo-photothermal therapy. *Adv Funct Mater* 28:1802830.
- Zhang H, Zhang J, Li Q, et al. (2020). Site-specific MOF-based immunotherapeutic nanoplatforms via synergistic tumor cells-targeted treatment and dendritic cells-targeted immunomodulation. *Biomaterials* 245:119983.
- Zheng Y, Zhao Y, Di Y, et al. (2019). DNA aptamers from whole-serum SELEX as new diagnostic agents against gastric cancer. *RSC Adv* 9: 950–7.
- Zhou J, Pishko MV, Lutkenhaus JL. (2014). Thermoresponsive layer-by-layer assemblies for nanoparticle-based drug delivery. *Langmuir* 30: 5903–10.
- Zhou K, Zhu Y, Chen X, et al. (2020). Redox- and MMP-2-sensitive drug delivery nanoparticles based on gelatin and albumin for tumor targeted delivery of paclitaxel. *Mater Sci Eng C* 114:111006.
- Zhu Z, Gong Y-B, Xu H-M. (2020). Neoadjuvant therapy strategies for advanced gastric cancer: current innovations and future challenges. *Chron Dis Transl Med* 6:147–57.